



## Single-grain OSL dating at La Grotte des Contrebandiers ('Smugglers' Cave'), Morocco: improved age constraints for the Middle Paleolithic levels

Z. Jacobs<sup>a,\*</sup>, M.C. Meyer<sup>a,b</sup>, R.G. Roberts<sup>a</sup>, V. Aldeias<sup>c</sup>, H. Dibble<sup>d,e,f</sup>, M.A. El Hajraoui<sup>g</sup>

<sup>a</sup> Centre for Archaeological Science, School of Earth and Environmental Sciences, University of Wollongong, Wollongong, NSW 2522, Australia

<sup>b</sup> Institute of Geology and Palaeontology, University of Innsbruck, Innrain 52, 6020 Innsbruck, Austria

<sup>c</sup> Department of Earth and Environmental Sciences, University of Pennsylvania, Philadelphia, PA 19104, USA

<sup>d</sup> Department of Anthropology, University of Pennsylvania, Philadelphia, PA 19104, USA

<sup>e</sup> Department of Human Evolution, Max Planck Institute for Evolutionary Studies, Deutscher Platz 6, Leipzig D-04103, Germany

<sup>f</sup> Institute of Human Origins, PO Box 872402, Arizona State University, Tempe, AZ 85287-2402, USA

<sup>g</sup> Institut National des Sciences de l'Archéologie et du Patrimoine, 10001 Rabat, Morocco

### ARTICLE INFO

#### Article history:

Received 7 May 2011

Received in revised form

24 August 2011

Accepted 25 August 2011

#### Keywords:

OSL dating

Single grains

Sand-sized quartz

Middle Paleolithic

Middle Stone Age

Morocco

Aterian

Moroccan Mousterian

Roof spall

Sediment mixing

Dose distributions

MIS 5

### ABSTRACT

Optically stimulated luminescence (OSL) measurements of individual quartz grains are reported for Middle Paleolithic (MP) or Middle Stone Age (MSA) deposits in La Grotte des Contrebandiers, Morocco. Single-grain measurements enable rejection of grains that may lead to under- or over-estimation of age due to malign luminescence properties or remobilisation of grains after burial. We identified the former using a range of experimental procedures and objective rejection criteria. Three post-depositional factors influenced the distribution pattern of equivalent dose ( $D_e$ ) values for the remaining single grains: the disintegration of roof spall liberating unbleached, older grains into otherwise well-bleached sediments; the intrusion of a small number of younger grains from the overlying Upper Paleolithic deposits; and small-scale differences in the beta dose received by individual grains. Roof spall contamination was a significant problem, so we characterised the OSL signals and obtained  $D_e$  values for the calcareous sandstone in which the cave is formed, which allowed bedrock-derived grains in the MP/MSA deposits to be identified and rejected prior to age determination. We collected 31 samples from the MP/MSA deposits, and were able to calculate ages for 30 of them. These ages suggest that MP/MSA occupation of Contrebandiers was restricted to the interval between about 120 and 90 ka ago (Marine Isotope Stages 5d to 5b). Weighted mean OSL ages were obtained for samples associated with archaeologically sterile deposits at the base of the excavations ( $126 \pm 9$  ka), followed by two phases of the Moroccan Mousterian ( $122 \pm 5$  and  $115 \pm 3$  ka), interspersed with archaeologically sterile deposits ( $112 \pm 4$  ka). The base and top of the Aterian were dated to  $107 \pm 4$  and  $96 \pm 4$  ka, respectively. Based on the grand weighted mean ages of  $116 \pm 3$  and  $103 \pm 3$  ka for the Moroccan Mousterian and Aterian at Contrebandiers, we suggest that these two industries may be separated by an occupation hiatus of up to  $13 \pm 3$  ka at this site. Our single-grain OSL chronology confirms previous age estimates obtained for Contrebandiers and other sites in the vicinity, but are generally more precise and stratigraphically more coherent, due to the inherent advantages of measuring individual quartz grains and rejecting contaminant and other unsuitable grains before age determination.

© 2011 Elsevier Ltd. All rights reserved.

### 1. Introduction

Morocco, in north-western Africa, is an important region for understanding the origins of anatomically modern humans, the emergence of cultural modernity and the dispersal of *Homo sapiens* within, and out of, Africa (Smith et al., 2007; Bouzouggar et al.,

2007; d'Errico et al., 2009; Richter et al., 2010). An increasing number of stratified sequences that contain human remains and objects of material culture attributed to the Middle and Upper Paleolithic are being investigated in Morocco, but many still lack reliable chronological control. La Grotte des Contrebandiers (hereafter referred to as Contrebandiers) is located on the Atlantic coast of Morocco and is one of few sites in North Africa known to contain evidence of human occupation extending from the Middle Paleolithic (MP) or Middle Stone Age (MSA) to the Neolithic. As

\* Corresponding author.

E-mail address: [zenobia@uow.edu.au](mailto:zenobia@uow.edu.au) (Z. Jacobs).

such, Contrebandiers has the potential to shed light on the nature and age of the two MP/MSA industries—the Mousterian and Aterian—and the succeeding Upper Paleolithic industry (the Iberomaurusian), and the transitions between them. In this paper, we are not concerned with the cultural definition of the artefact assemblages—the cultural attributions of individual levels, and correlations between assemblages from different sites, are the subject of papers in preparation and of new studies that are underway. Here we address the chronological question, for which a key requirement is an accurate and precise numerical chronology for the archaeological sequence. Existing chronologies for the site are poorly constrained. Radiocarbon ( $^{14}\text{C}$ ) dating of shell, bone and soil samples from the MP/MSA levels produced uncalibrated ages as young as  $\sim 12$  ka BP to  $>35$  ka BP (Delibrias et al., 1982), while uranium-series dating of shell gave two ages consistent with the last interglacial ( $\sim 125$  ka) (Roche, 1976). More recently, 10 sediment samples from the MP/MSA levels were dated by optically stimulated luminescence (OSL), using sub-samples composed of many (50–150) grains of quartz, resulting in ages of between  $59 \pm 10$  and  $129 \pm 7$  ka (Schwenninger et al., 2010).

In this paper, we present the results of an OSL dating study of samples collected from secure stratigraphic and archaeological contexts during archaeological excavations at Contrebandiers conducted recently by H. Dibble and M. El Hajraoui. OSL dating provides an estimate of the time since grains of quartz or feldspar were last exposed to sunlight. After burial, environmental sources of ionising radiation supply energy to the grains, resulting in the generation of a palaeodose, which can be measured in the laboratory using the OSL signal to obtain an estimate of the equivalent dose ( $D_e$ ). The  $D_e$  is divided by the environmental dose rate to estimate the burial age of the grains. We used single-grain OSL techniques in preference to multi-grain dating procedures (such as those used by Schwenninger et al., 2010), so that  $D_e$  values could be obtained from individual grains of sand-sized quartz. A single grain is the smallest meaningful unit of measurement in OSL dating, insofar as each grain may have a different history of solar bleaching and subsequent burial. From single-grain measurements, OSL ages can be determined with improved accuracy and precision, because contaminant grains can be identified and discarded before age determination (e.g., Roberts et al., 1998; Jacobs et al., 2003b, 2006b, 2008a,c; Feathers et al., 2006a,b, 2010; Porat et al., 2006), as can grains with aberrant physical characteristics that make them unsuitable for dating (e.g., Roberts et al., 1999; Yoshida et al., 2000; Jacobs et al., 2003b, 2006a,b). Hundreds or thousands of individual grains can be measured efficiently with existing instrumentation, generating a statistically significant number of  $D_e$  values that can be examined using a variety of well-established statistical models to determine a reliable age (e.g., Galbraith et al., 1999; Roberts et al., 2000; David et al., 2007; Olley et al., 2006; Jacobs et al., 2008a,c).

Over the last decade, much effort has been devoted to developing improved methods to measure  $D_e$  values for individual grains of quartz, and to understand and interpret the resulting  $D_e$  distributions (Jacobs and Roberts, 2007). A common feature of archaeological sediments is the large amount of spread, commonly referred to as 'overdispersion', observed between the true  $D_e$  values of grains from the same sample. Overdispersion is a quantitative estimate of the amount of spread in the  $D_e$  data set after allowance has been made for measurement uncertainties (Galbraith et al., 1999; Roberts et al., 2000). At archaeological sites,  $D_e$  overdispersion may reflect the post-depositional intrusion of younger or older grains by natural processes or anthropogenic activities (e.g., Bateman et al., 2003, 2007a,b; Feathers et al., 2006a,b, 2010; Jacobs et al., 2006b, 2008a; David et al., 2007; Marean et al., 2007; Porat et al., 2006; Lombard et al., 2010; Tribolo et al., 2010), the *in situ* breakdown of unbleached roof spall in

otherwise well-bleached sediments (e.g., Roberts et al., 1998, 1999), inhomogeneous or partial resetting of the OSL signal prior to burial (e.g., Olley et al., 1999, 2004, 2006; Duller and Murray, 2000; Duller et al., 2000; Murray and Olley, 2002), and/or the effects of variations in the beta dose received by individual grains of sand (e.g., Murray and Roberts, 1997; Olley et al., 1997; Roberts et al., 1999; Jacobs et al., 2008a,c; Haslam et al., 2011). To discriminate between these possibilities, the extent of overdispersion is routinely quantified and the  $D_e$  distributions are examined visually to discern any patterns in the data. The radial plot (Galbraith, 1988) simultaneously provides information about the spread in  $D_e$  values, their precisions and their statistical consistency, thereby facilitating the recognition of any patterns and their possible causes (Galbraith et al., 1999; Jacobs and Roberts, 2007).

All such assessments of a sample's bleaching and post-depositional history should take into account its sedimentary and archaeological context to select the most appropriate statistical model for final  $D_e$  and age determination. In the case of post-depositional sediment mixing and roof spall contamination, only single-grain OSL dating can reveal the true structure of the underlying  $D_e$  distribution (Arnold and Roberts, 2009). Single-grain analysis has the potential, therefore, to substantially improve our understanding of  $D_e$  overdispersion in archaeological settings and assist in the selection of the most appropriate statistical model for age determination. It can also help shed light on the stratigraphic integrity of a site and its archaeological assemblage. We have applied this approach to the MP/MSA deposits at Contrebandiers.

The first part of this paper provides the stratigraphic and archaeological contexts of the OSL dating samples from Contrebandiers. The second part of the paper reports the  $D_e$  distributions, focussing on those aspects that influence the spread of  $D_e$  values. We combine our knowledge of the site context with the observed distribution pattern of  $D_e$  values to explain the latter and decide on the most appropriate statistical model to use for age estimation. Worked examples of the dating procedures used in this study are provided in Supplementary Material, along with information about the measurement procedures used to obtain reliable  $D_e$  estimates, the luminescence properties of individual quartz grains, and the reasons for rejecting unsuitable grains. In the final part of the paper, we provide information on environmental dose rates and OSL ages, concluding with a discussion of the implications for the antiquity and duration of MP/MSA occupation of Contrebandiers.

## 2. Site setting, stratigraphy and archaeological context

Contrebandiers is located along the Tèmara coast of Morocco,  $\sim 270$  m inland from the Atlantic Ocean with the top of the Pleistocene deposits situated  $\sim 11$  m above current sea level (Fig. 1). The cave is cut into a  $\sim 5$  m-high cliff composed of massive calcareous sandstone, with occasional bedding planes dipping  $5$ – $10^\circ$  north-northeast to southeast. The cave has a total length of  $\sim 33$  m, a frontal opening up to  $\sim 3$  m in height (Fig. 2b), and a roof  $2$ – $3.5$  m in thickness. Numerous dissolution features occur inside the cave, such as ceiling pockets and a phreatic tunnel at the back of the cave, a chimney (now filled with concrete) also at the rear of the cave, and a few remnant flowstone formations composed of brownish and very porous calcite. Active speleothem formation is restricted to a few small ( $<5$  cm long) soda straws. The age and exact process of cave formation are not known, but erosion by waves during phases of high sea level was probably important. The formation of Contrebandiers, and the numerous nearby caves that occur in similar settings, might correspond, therefore, to one of the Pleistocene interglacials.

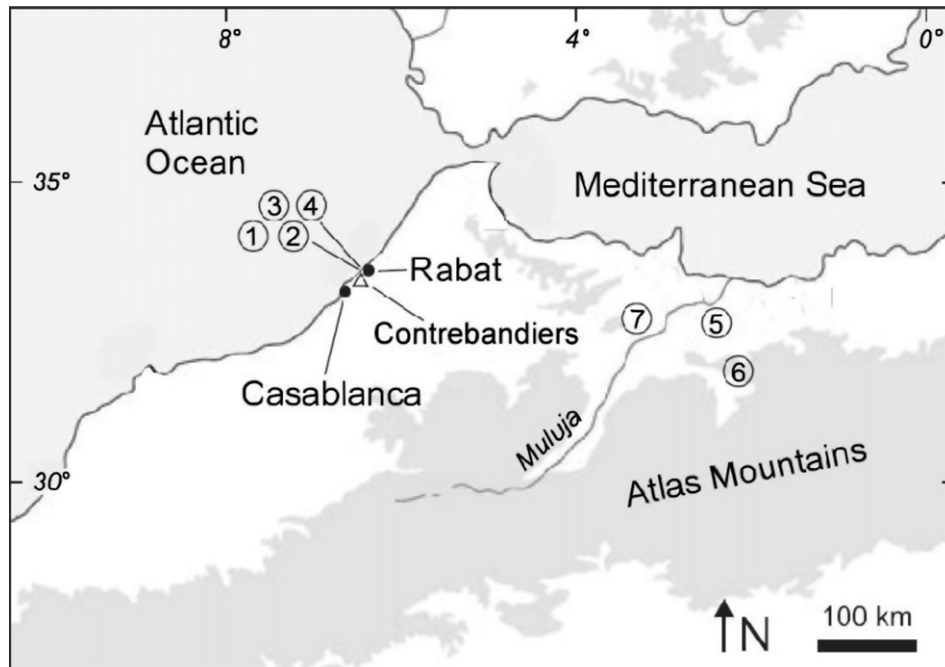


**Fig. 1.** Map of north-western Africa indicating some of the better known Middle Paleolithic sites in Morocco: El Mnasra (1), El Harhoura 2 (2), Dar es-Soltan 1 and 2 (3 and 4), Taforal (5), Rhafas (6), Ifri n'Ammar (7). La Grotte des Contrebandiers is indicated with an open triangle.

The site was first discovered in 1955 by A.J. Roche and has since been the subject of repeated archaeological investigations (Roche, 1958–1959, 1963, 1976; Roche and Texier, 1976; Bouzouggar, 1997a,b; Schurmans et al., 2007, 2009). Each new group of excavators described a new stratigraphy for the site, so correlation between the different schemes is not straightforward. The current excavations have established a correlation with the previous stratigraphic sequence proposed by Roche (see section below titled 'Age estimates and discussion'). All groups, however, agree that Contrebandiers contains an archaeological record consisting of so-called Mousterian, Aterian, Iberomaurusian and Neolithic assemblages. Except for the Iberomaurusian, the archaeology remains largely unpublished, but a comprehensive account of the current excavations is in progress. The site has also yielded important human remains from the Aterian levels (e.g., Ferembach, 1976, 1998; Hublin, 1992, 1993; Debénath, 2000). Several teeth, partly attached to the maxillary fragment, were recovered from the Iberomaurusian levels (Ménard, 1998), while a mandible, an occipital and a frontal fragment were found in proximity to each other, associated with Aterian assemblages (Roche and Texier, 1976). Additional skeletal remains have also been recovered recently from the underlying Moroccan Mousterian levels (Balter, 2011).

Fig. 2a shows a planform map of the cave on which the positions of five excavation Sectors are indicated. These five Sectors correspond to the current excavations directed by H. Dibble and M. El Hajraoui. The stratigraphy in Sectors I, II and III are now correlated and are divided into seven archaeological layers, labelled 1–7 from top to bottom. This area is now referred to as the central excavation area and it is mostly correlated with the profile visible in the existing Roche Trench, from which the majority of the OSL samples reported in Schwenninger et al. (2010) were collected. Sectors IV and V each consist of two archaeological layers (designated by the prefix IV- and V-, respectively, followed by the number of the layer), but these remain uncorrelated to the other Sectors. Thus, layer IV-2 (from Sector IV) is independent from layer V-2. Neolithic deposits have not been found in any of these Sectors, except in the form of

a few infilled pits. The Neolithic has been almost completely removed from Contrebandiers by previous excavators and is now restricted to remnants along the southeastern and northern cave walls. Iberomaurusian deposits were found in a small portion of Sector IV. The Aterian is present in the upper layers of the central excavation area, the basal layer of Sector IV and in Sector V. The Moroccan Mousterian has been reached only in the central excavation area. The cave-mouth deposits in the central excavation area have been excavated to a depth of ~4 m, where bedrock was encountered. Table 1 provides a breakdown of the different Sectors, archaeological layers and associated archaeological industries as determined by the current excavation team, in addition to the locations of the OSL dating samples.

### 3. OSL dating samples

Thirty-three samples were collected for OSL dating from the Aterian, Moroccan Mousterian and archaeologically sterile layers in the central excavation area and Sectors IV and V in 2007, 2008 and 2010 by hammering opaque plastic tubes (6 cm in diameter and 15 cm in length) into the cleaned section walls. Samples were also collected from the Upper Paleolithic and Neolithic levels, but the results for those will be reported separately elsewhere. Additional material was collected from each sample location for laboratory-based measurements of radioactivity and field moisture content. At least one sample was collected from each stratigraphic layer, and relatively thick layers were sampled at the top and bottom to obtain bracketing ages. Fig. 3 shows the positions of 28 of the OSL samples in their sedimentary contexts.

Nearly half of the samples ( $n = 14$ ) were collected from two adjacent squares and sediment profiles in the central excavation area. Fig. 3a shows the locations of 12 of these samples. The samples from square J19 (Figs. 2a and 3a) were collected in 2007 by the excavation team, but no *in situ* gamma spectrometry measurements were made. By the time the OSL dating team arrived at the site in 2008, the majority of square J19 had already been excavated,

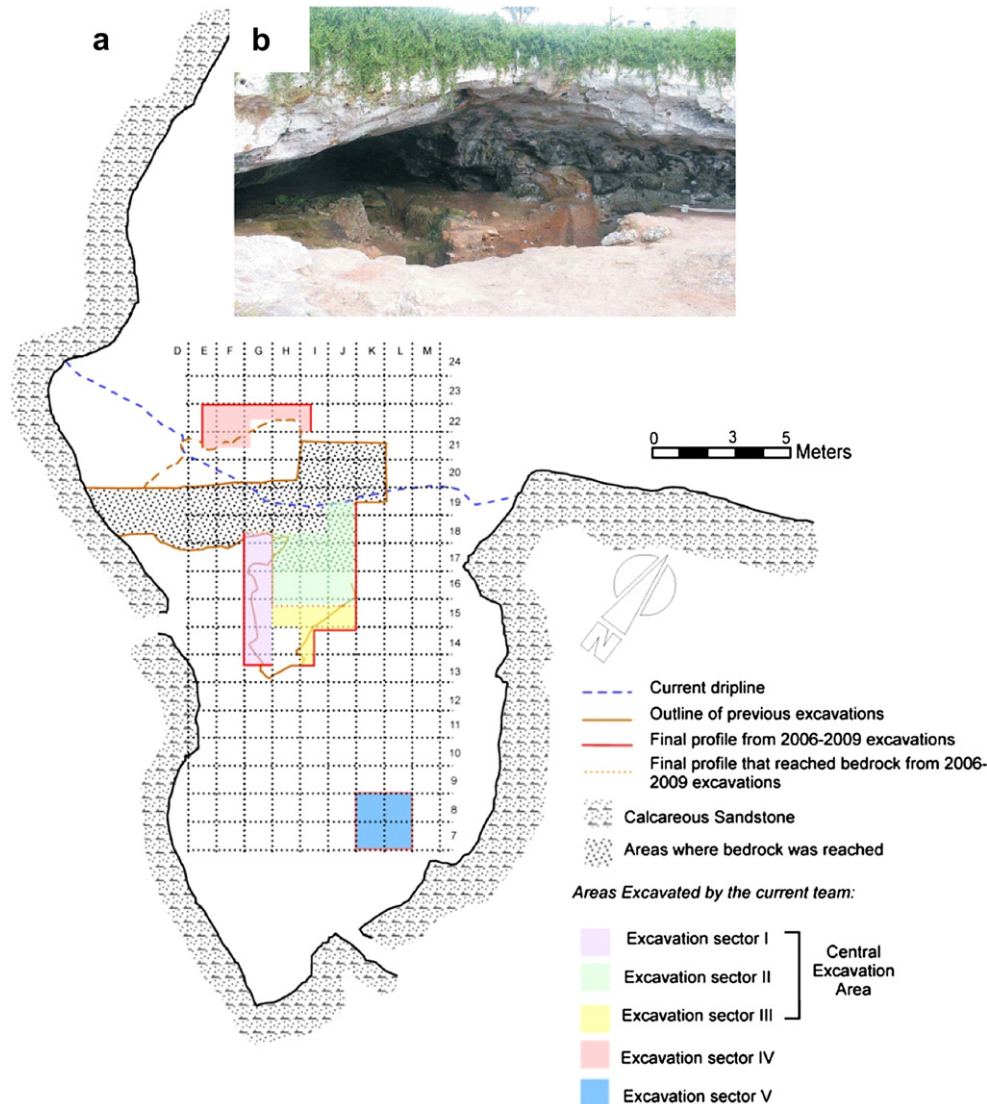


**Fig. 2.** a) Planform map of the cave, showing the excavation Sectors discussed in the text. b) Photograph of the opening of Contrebandiers, cut into calcareous sandstone.

so we sampled the adjacent square (K19) and made *in situ* measurements of the gamma dose rate, to check whether the OSL ages are sensitive to the determination of the gamma dose rate by field or laboratory techniques. All samples collected from these two squares are associated with either the Moroccan Mousterian

(archaeological layers 5a–c and 6c) or archaeologically sterile sediments (layers 6a/b and 7). No sediments associated with the Aterian were found in either square.

We also collected samples laterally from the same layers but from different squares, to investigate the temporal and spatial

**Table 1**  
Summary of the different excavation areas and a breakdown of the archaeological layers and industries associated with them. Also listed are the OSL samples collected from each of the layers and Sectors, for comparison with Figs. 2a and 3.

Central excavation area and Roche's Trench (RT)			Sector IV			Sector V		
Layer	Archaeological industries	OSL sample	Sector-layer	Archaeological industries	OSL sample	Sector-layer	Archaeological industries	OSL sample
			IV-1a	Iberomaurusian		V-1a	Aterian	
			IV-1b	Iberomaurusian		V-1b	Aterian	SC23
			IV-2a	Aterian	SC30, SC39	V-2	Aterian	SC34
			IV-2b	Aterian	SC37			
RT-4 upper	Aterian	SC31, SC32						
4	Aterian	SC7, SC8, SC20, SC21, SC35						
5a	Mousterian	SC16						
5b	Mousterian	SC15						
5c	Mousterian	SC1, SC6, SC13, SC14,						
5c	Mousterian	SC19, SC28, SC2						
6a/b	Sterile	SC3, SC12, SC18, SC29						
6c	Mousterian	SC4, SC10, SC11, SC17						
7	Sterile	SC5, SC9						

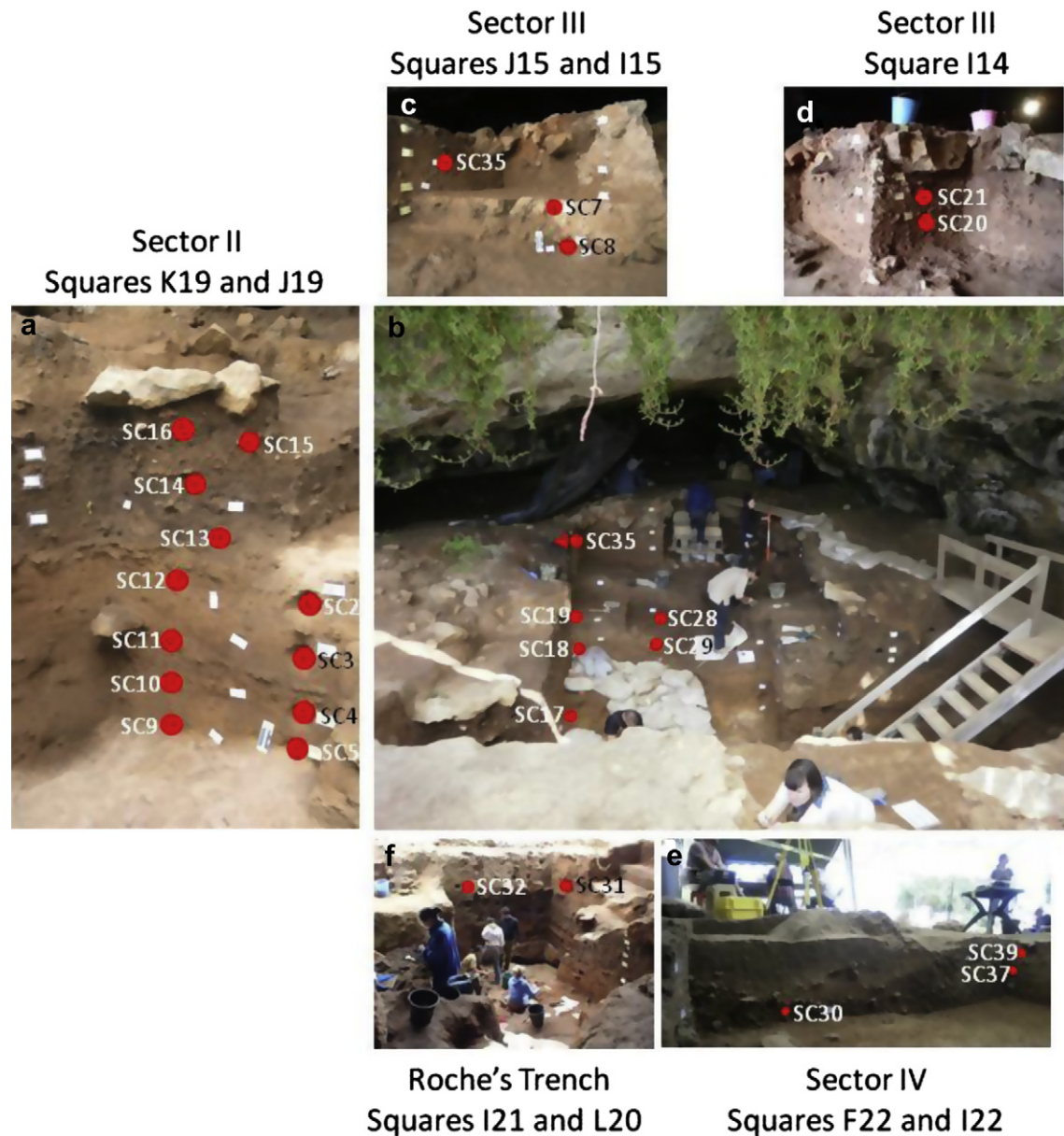


**Fig. 3.** Photographs showing section walls in the squares and Sectors from which OSL samples were collected. The positions of 27 of the samples are indicated on the photographs. The two bedrock samples (SC22 and SC26), and the two samples collected from Sector V (SC23 and SC34) in the back of the cave, are not shown. SC1 and SC6 were excavated before these photographs were taken, but both were collected just above SC2 in photo (a).

relationship of the sediments, and to obtain ages in proximity to the human skull discovered in 2009 in square I15 (Fig. 2a). The locations of these OSL samples are shown in sedimentary context in Fig. 3b. Samples associated with the Aterian were collected from four different areas in the cave: layer 4 in the central excavation area (Fig. 3b–d), layer IV-2 in Sector IV (Fig. 3e), layers V-1 and V-2 in Sector V, and the upper deposits in Roche's original trench (Fig. 3f). We also collected two samples of calcarenite bedrock, one from a cemented sand unit at the base of square K20 in the central excavation area (SC26) and the other from the wall immediately outside the cave entrance (SC22). Both samples are indicative of a depositional environment at the beach shore.

For OSL dating, quartz grains were chemically extracted from the bulk sediment samples and grains of 180–212  $\mu\text{m}$  in diameter were selected for OSL dating. Details about sample preparation, OSL equipment and measurement and data analysis procedures,

including the reasons for rejecting unsuitable grains, are provided in full in Supplementary Material. Also provided is a synopsis of the luminescence properties of the quartz grains.

#### 4. $D_e$ distributions and interpretations

Of the 24,000 individual sand-sized grains of quartz measured (excluding the 2700 grains from the bedrock samples), 3921 grains (16.3% of the total number of grains measured) were used for final  $D_e$  determination. The  $D_e$  values for these grains are displayed as radial plots in Fig. S5 for each of the samples, including the two bedrock samples. In such plots, the most precise estimates fall to the right and the least precise to the left. If these independent estimates are consistent with statistical expectations, then 95% of the points should scatter within a band of width  $\pm 2$  units projecting from the left-hand ('standardised estimate') axis to any chosen  $D_e$  value on

the right-hand, radial axis. To facilitate direct comparison of the single-grain  $D_e$  values between samples, the radial axis scale has been kept constant in Fig. S5. It is immediately apparent from these plots that, for each of the samples, the  $D_e$  estimates are spread too widely to fall within any single band of  $\pm 2$  units. This is also reflected in the  $D_e$  overdispersion values (Table 2), which range from  $21 \pm 3\%$  (SC18) to  $54 \pm 4\%$  (SC31), and are much greater than the 0% overdispersion obtained for sample SC3 under controlled laboratory conditions in a dose recovery test (Fig. S2).

A number of field-related processes may increase the spread in  $D_e$  values for these samples, so understanding why and how these processes affect single-grain  $D_e$  distributions is critical to obtaining accurate OSL age estimates. Aeolian and littoral sedimentation have been the prevailing depositional processes at Contrebandiers. Given the prolonged sunlight exposure that sediments typically receive when transported by such processes, it is reasonable to assume that their OSL signals were reset to zero, or nearly so. However, there is an open sink hole and a phreatic tunnel at the back of Contrebandiers, and it is possible that soil and sediment from the surface were occasionally washed into the shallow cave via these openings, or through fissures in the shallow roof, resulting in grains that might have been bleached incompletely or heterogeneously before deposition.

Post-depositional modification of sediments is quite common in Contrebandiers. The Aterian and Mousterian levels have, in places,

been affected by anthropogenic disturbance, in the form of Neolithic pits. Evidence of bioturbation by burrowing small mammals and insects can also be observed in some of the sediment profiles. Such anthropogenic and natural disturbances can result in the mixing of grains of different ages, and the introduction of modern, light-exposed grains into the older sediments.

Laterally extensive carbonate crusts also occur throughout the deposits (e.g., Fig. S6a). These crusts are interpreted as cementation features caused by drip-water activity during, or shortly after, deposition of the cave-mouth sediments. In some instances, entire sediment patches are cemented by secondary carbonates. Thick carbonate crusts have also formed around many of the bones, shells and stones in the archaeological layers, and had to be removed with hydrochloric acid prior to analysis. The common occurrence of carbonate and its inhomogeneous distribution may affect the beta dose rate received by individual grains on both spatial and temporal scales, because carbonate is radioactively inert compared to most other minerals. The two samples of calcareous sandstone bedrock, for example, have much lower dose rates than do the archaeological sediments (Table 2). Quartz grains that are partly or completely surrounded by more than 2 mm of carbonate will, therefore, have experienced a lower beta dose rate than grains that were deposited at the same time but were not affected subsequently by carbonate cementation, resulting in smaller  $D_e$  values. The opposite is true for grains that are surrounded or juxtaposed by bones and shells,

**Table 2**  
Dose rate data,  $D_e$  values and OSL ages for 33 sediment samples from Contrebandiers. The  $D_e$  of sample SC22 was determined using the central age model (CAM) because the two discrete dose components identified by the finite mixture model (FMM) were present in approximately equal proportions.

Sample name	Moisture content (%)	Dose rate (Gy/ka)				Number of grains accepted/measured	Age model	Overdispersion (%)	$D_e$ value (Gy)	Age (ka)
		Beta	Gamma	Cosmic	Total					
Aterian (layer 4 in the central excavation area and the Roche Trench, layer V-1b and V-2 in Sector V and layer IV-2 in Sector IV)										
SC30	9.9	$0.56 \pm 0.03$	$0.34 \pm 0.03$	$0.13 \pm 0.01$	$1.06 \pm 0.07$	197/800	FMM	$48 \pm 3$	mixed	
SC39	5.8	$0.40 \pm 0.03$	$0.34 \pm 0.03$	$0.14 \pm 0.01$	$0.92 \pm 0.06$	138/500	FMM	$46 \pm 4$	$88.3 \pm 3.3$	$96 \pm 8$
SC37	9.9	$0.57 \pm 0.04$	$0.40 \pm 0.03$	$0.14 \pm 0.01$	$1.13 \pm 0.07$	196/1000	FMM	$44 \pm 3$	$114.8 \pm 6.9$	$101 \pm 9$
SC31	2.2	$0.62 \pm 0.04$	$0.47 \pm 0.03$	$0.11 \pm 0.01$	$1.23 \pm 0.07$	142/700	FMM	$54 \pm 4$	$113.2 \pm 4.8$	$92 \pm 6$
SC32	7.3	$0.64 \pm 0.04$	$0.47 \pm 0.04$	$0.13 \pm 0.01$	$1.27 \pm 0.08$	215/1000	FMM	$33 \pm 2$	$123.2 \pm 5.1$	$97 \pm 7$
SC21	10.7	$0.57 \pm 0.03$	$0.34 \pm 0.01$	$0.09 \pm 0.01$	$1.04 \pm 0.05$	111/700	FMM	$32 \pm 3$	$106.7 \pm 3.1$	$103 \pm 6$
SC35	8.8	$0.62 \pm 0.04$	$0.44 \pm 0.03$	$0.09 \pm 0.01$	$1.18 \pm 0.07$	231/1000	FMM	$33 \pm 3$	$124.1 \pm 7.3$	$105 \pm 9$
SC20	14.2	$0.75 \pm 0.04$	$0.38 \pm 0.01$	$0.09 \pm 0.01$	$1.26 \pm 0.06$	74/700	FMM	$27 \pm 3$	$130.4 \pm 4.9$	$104 \pm 7$
SC8	6.9	$0.47 \pm 0.03$	$0.35 \pm 0.01$	$0.09 \pm 0.01$	$0.94 \pm 0.05$	52/500	CAM	$32 \pm 4$	$101.7 \pm 5.4$	$108 \pm 9$
SC7	3.2	$0.59 \pm 0.03$	$0.39 \pm 0.01$	$0.10 \pm 0.01$	$1.11 \pm 0.06$	74/700	FMM	$36 \pm 4$	$130.0 \pm 5.9$	$117 \pm 9$
SC23	10.3	$0.77 \pm 0.03$	$0.29 \pm 0.01$	$0.09 \pm 0.01$	$1.18 \pm 0.05$	69/700	FMM	$27 \pm 3$	$133.0 \pm 5.2$	$113 \pm 7$
SC34	20.6	$0.79 \pm 0.05$	$0.34 \pm 0.01$	$0.09 \pm 0.01$	$1.25 \pm 0.07$	262/1000	FMM	$39 \pm 2$	$133.4 \pm 7.2$	$107 \pm 9$
Moroccan Mousterian (layers 5a–c)										
SC16	20.6	$0.52 \pm 0.03$	$0.29 \pm 0.01$	$0.11 \pm 0.01$	$0.95 \pm 0.04$	92/800	FMM	$31 \pm 3$	$112.6 \pm 5.9$	$118 \pm 9$
SC15	22.5	$0.53 \pm 0.03$	$0.30 \pm 0.01$	$0.11 \pm 0.01$	$0.97 \pm 0.05$	73/700	FMM	$38 \pm 4$	$112.6 \pm 5.0$	$116 \pm 8$
SC19	18.7	$0.40 \pm 0.02$	$0.25 \pm 0.01$	$0.09 \pm 0.01$	$0.78 \pm 0.04$	176/800	FMM	$40 \pm 3$	$97.4 \pm 4.5$	$124 \pm 9$
SC14	24.3	$0.43 \pm 0.02$	$0.31 \pm 0.01$	$0.11 \pm 0.01$	$0.88 \pm 0.04$	148/800	FMM	$37 \pm 3$	$99.6 \pm 2.9$	$113 \pm 7$
SC6	10.5	$0.55 \pm 0.04$	$0.36 \pm 0.01$	$0.10 \pm 0.01$	$1.04 \pm 0.06$	106/700	FMM	$28 \pm 3$	$118.5 \pm 3.9$	$114 \pm 8$
SC13	18.2	$0.52 \pm 0.03$	$0.33 \pm 0.01$	$0.10 \pm 0.01$	$0.99 \pm 0.05$	84/900	FMM	$23 \pm 3$	$110.4 \pm 3.4$	$112 \pm 7$
SC1	6.8	$0.48 \pm 0.03$	$0.34 \pm 0.01$	$0.10 \pm 0.01$	$0.95 \pm 0.06$	87/500	FMM	$33 \pm 3$	$108.6 \pm 3.5$	$115 \pm 8$
SC28	22.8	$0.57 \pm 0.04$	$0.45 \pm 0.01$	$0.09 \pm 0.01$	$1.14 \pm 0.06$	148/900	FMM	$42 \pm 3$	$130.5 \pm 5.6$	$115 \pm 8$
SC2	17.2	$0.66 \pm 0.04$	$0.45 \pm 0.02$	$0.10 \pm 0.01$	$1.24 \pm 0.07$	134/500	FMM	$36 \pm 3$	$140.8 \pm 6.3$	$114 \pm 8$
Archaeologically sterile (layers 6a/b)										
SC18	19.5	$0.61 \pm 0.04$	$0.38 \pm 0.01$	$0.09 \pm 0.01$	$1.11 \pm 0.06$	76/800	FMM	$21 \pm 3$	$126.4 \pm 3.9$	$114 \pm 6$
SC29	24.6	$0.70 \pm 0.04$	$0.39 \pm 0.02$	$0.09 \pm 0.01$	$1.21 \pm 0.07$	230/1000	FMM	$40 \pm 2$	$131.9 \pm 4.6$	$109 \pm 7$
SC12	16.1	$0.59 \pm 0.03$	$0.35 \pm 0.01$	$0.10 \pm 0.01$	$1.08 \pm 0.05$	151/1000	FMM	$40 \pm 3$	$127.8 \pm 5.8$	$119 \pm 8$
SC3	16.5	$0.62 \pm 0.04$	$0.43 \pm 0.02$	$0.10 \pm 0.01$	$1.19 \pm 0.07$	96/500	FMM	$38 \pm 4$	$126.6 \pm 6.1$	$107 \pm 8$
Moroccan Mousterian (layer 6c)										
SC11	16.9	$0.59 \pm 0.03$	$0.33 \pm 0.01$	$0.10 \pm 0.01$	$1.05 \pm 0.05$	207/1100	FMM	$43 \pm 3$	$127.7 \pm 6.3$	$122 \pm 9$
SC17	12.5	$0.52 \pm 0.03$	$0.34 \pm 0.01$	$0.08 \pm 0.01$	$0.98 \pm 0.05$	114/800	FMM	$27 \pm 3$	$116.3 \pm 3.0$	$119 \pm 7$
SC4	17.8	$0.50 \pm 0.03$	$0.36 \pm 0.01$	$0.10 \pm 0.01$	$0.99 \pm 0.06$	125/500	FMM	$33 \pm 3$	$118.5 \pm 3.4$	$120 \pm 8$
SC10	18.7	$0.51 \pm 0.03$	$0.30 \pm 0.01$	$0.09 \pm 0.01$	$0.94 \pm 0.05$	126/700	FMM	$31 \pm 3$	$121.9 \pm 5.0$	$130 \pm 9$
Archaeologically sterile (layer 7)										
SC5	7.4	$0.28 \pm 0.02$	$0.20 \pm 0.01$	$0.09 \pm 0.01$	$0.61 \pm 0.03$	37/900	FMM	$38 \pm 6$	$75.1 \pm 5.7$	$123 \pm 11$
SC9	7.4	$0.27 \pm 0.02$	$0.20 \pm 0.01$	$0.09 \pm 0.01$	$0.59 \pm 0.03$	102/800	FMM	$24 \pm 3$	$78.1 \pm 7.7$	$132 \pm 15$
Bedrock (calcareous sandstone)										
SC26	0.1	$0.15 \pm 0.01$	$0.13 \pm 0.01$	$0.09 \pm 0.01$	$0.40 \pm 0.02$	46/1100	FMM	$39 \pm 6$	$197.2 \pm 12.3$	$421 \pm 37$
SC22	0.1	$0.18 \pm 0.01$	$0.15 \pm 0.01$	$0.13 \pm 0.01$	$0.48 \pm 0.03$	76/1600	CAM	$37 \pm 4$	$164.2 \pm 8.5$	$341 \pm 27$

which are notorious for soaking up uranium from percolating groundwater, thereby exposing those grains to higher-than-average beta dose rates.

Finally, cave-mouth deposits commonly contain some amount of roof spall. The *in situ* disintegration of spalled chunks or clasts will liberate unbleached or partially bleached quartz grains into the archaeological sediments. If such grains are not detected and removed from the  $D_e$  data set before calculating the sample age, then the latter may be substantially overestimated (e.g., Roberts et al., 1998, 1999).

To decipher which, if any, of these factors may have caused the observed spread in  $D_e$  values for the samples from Contrebandiers (Fig. S5), the central age model (CAM) and finite mixture model (FMM) were systematically applied to all single-grain  $D_e$  distributions, in conjunction with knowledge of the sedimentary contexts of the samples. The FMM was used to determine if a  $D_e$  distribution consisted of a number of discrete components and, if so, to estimate the relative proportion of grains in each component and the weighted mean  $D_e$  value and associated standard error of each component (Roberts et al., 2000; David et al., 2007; Jacobs et al., 2008b). A worked example explaining how we implemented the FMM and interpreted the results is provided in Supplementary Material. We ran the FMM using overdispersion values of between 10 and 20% and identified the minimum number of statistically supported  $D_e$  components by means of maximum log likelihood and the Bayes Information Criterion (BIC). Each  $D_e$  distribution in Fig. S5 is annotated with the discrete components identified by the FMM (for the smallest BIC), either as a grey line or a grey shaded band of width  $\pm 2$  units centred on the weighted mean  $D_e$  value for that component. Also shown is the estimated percentage of grains in each  $D_e$  component.

Three general patterns can be observed in these radial plots, and all three patterns are present in the  $D_e$  distributions of several samples, including SC31 (Fig. 4). First, many of the samples have a high  $D_e$  component centred on a value of between 200 and 300 Gy. These are considered to be contaminant grains, derived from disintegrated and unbleached roof spall. Second, a few samples have a low- $D_e$  component centred on a value of between 14 and 37 Gy. These are thought to be intrusive grains from the overlying Upper Paleolithic levels. Third, the majority of single-grain  $D_e$  values in all samples fall into one or two discrete components, but a few values also fall between these two components. These  $D_e$  distributions are typical of samples composed of grains that have the same burial age, but that were exposed to different beta dose rates after burial, owing to the inhomogeneity of the sediments (Jacobs et al., 2008a). The identification, impact and treatment of each of these depositional and post-depositional factors are discussed below.

#### 4.1. Contamination by roof spall

In most cases where samples from cave sites have been examined, the age of the bedrock is considerably greater (e.g., millions of years older) than that of the archaeological deposit, so any quartz grains derived from roof spall have natural OSL signals that are fully saturated in respect to radiation dose (e.g., Roberts et al., 1999; Jacobs et al., 2006b). Such grains are rejected during single-grain analysis, because a  $D_e$  value cannot be obtained for grains with sensitivity-corrected natural signals that approach or exceed the sensitivity-corrected regenerated signals at high applied doses. At Contrebandiers, however, preliminary tests on the two bedrock samples (SC22 and SC26; Table 2) suggested that the calcareous sandstone in which the cave formed may be of Middle Pleistocene age. If roof spall contamination of the archaeological sediments is a problem at Contrebandiers, then these grains might have large

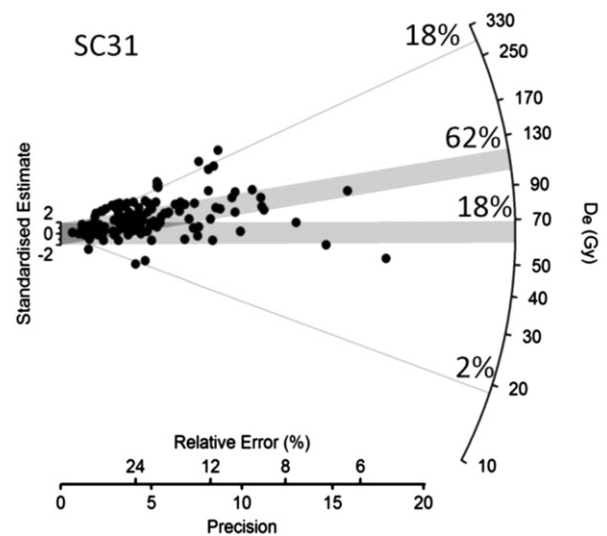


**Fig. 4.** Example of a  $D_e$  distribution for one of the Contrebandiers samples (SC31) that shows evidence of all three post-depositional processes discussed in the text. The distribution pattern of  $D_e$  values displayed in this radial plot is consistent with 4 separate populations of grains, as determined using the FMM (see Table S2). The grey lines and shaded bands are centred on the weighted mean  $D_e$  values of each population, and the percentage of grains contained in each population is indicated. The grey lines show the two populations of grains identified as being intrusive, while the shaded bands show the two components that are considered to consist of grains deposited at the same time, but which subsequently received variable beta doses. The major component (62% of the grains in this example) was used for sample  $D_e$  and age determination, after adjusting the beta dose rate as described in Supplementary Material.

but finite  $D_e$  values. It is necessary, therefore, to determine the characteristic  $D_e$  values of the quartz grains from the host rock, so that they can be identified and removed from the  $D_e$  distributions of the archaeological sediments before calculating their ages.

More than 1000 individual quartz grains from each of samples SC22 and SC26 were measured using the same procedures as described above for the archaeological sediments. After application of the standard rejection criteria, only 4–5% of the grains were suitable for estimation of  $D_e$ . The calculated overdispersion values for both samples were surprisingly large,  $37 \pm 4\%$  for SC22 and  $39 \pm 6\%$  for SC26 (Table 2), which is reflected in the wide spread of  $D_e$  values shown in Fig. 5. Two discrete  $D_e$  components can be fitted to both data sets using the FMM. For sample SC22, collected from outside the cave, the two components are present in approximately equal proportions (Fig. 5a). The range of  $D_e$  values can be explained by the spatially inhomogeneous beta dose rate received by individual grains as a result of the coarse-grained, porous nature of the rock and the presence of shell fragments, which were noticed when this sample was disaggregated in the laboratory for pretreatment.

For sample SC26 (collected from the base of the central excavation area), the majority of grains (78%) fall in the higher  $D_e$  component and the minor component consists of grains with  $D_e$  values that are too small to be explained solely as a function of greatly reduced beta dose rates (Fig. 5b) (see Supplementary Material and Jacobs et al., 2008a,b). Like SC22, sample SC26 is composed of yellowish coarse sand with fragments of marine mollusc shell. The surface of the bedrock from which SC26 was collected is irregular, due mainly to bioturbation. Burrow structures, in the form of a dense but irregular network of tubes up to 6 cm in diameter, are common and the larger tubes are typically filled with uncemented reddish sand, which may be the source of the grains that constitute the low- $D_e$  component in Fig. 5b. When these contaminant grains are removed from the data set, the

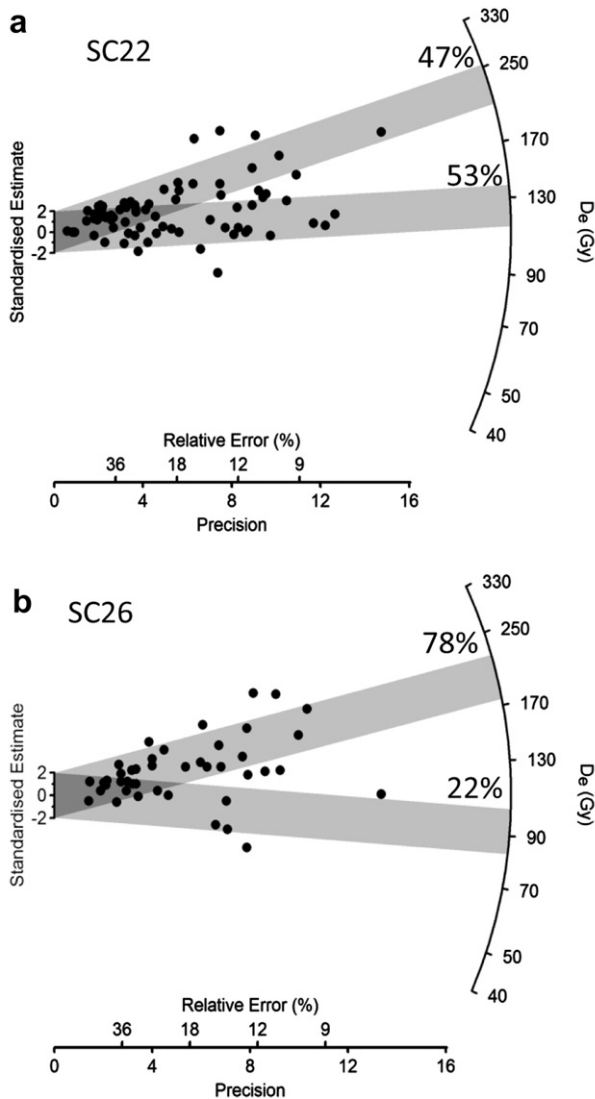


**Fig. 5.** Radial plots showing the single-grain  $D_e$  values obtained for the two bedrock samples collected from the calcareous sandstone (a) outside the cave (SC22) and (b) inside the cave at the base of the central excavation area (SC26). As in Fig. 4, the grey bands are centred on the weighted mean  $D_e$  values of the 2 identified components and the percentage of grains in each component is also indicated.

overdispersion value for SC26 shrinks to  $23 \pm 5\%$  and the  $D_e$  distribution can be adequately fitted by a single component with  $D_e$  values that are symmetrically distributed around a weighted mean of  $\sim 200$  Gy (Table 2). The  $D_e$  values for sample SC22 are also spread, albeit more broadly, about a similar mean value.

Before comparing the  $D_e$  distributions of the bedrock and MP/MSA samples, it is necessary to consider the different dose rates to which these grains have been exposed. The two bedrock samples have total dose rates of 0.4–0.5 Gy/ka, whereas the archaeological sediments (except those from sterile layer 7) have total dose rates more than double that, ranging from  $\sim 0.8$  to  $\sim 1.3$  Gy/ka (Table 2). If roof spall grains are present as contaminants in the archaeological deposit, then their  $D_e$  values will depend on when the spalled grains were incorporated into the archaeological sediment matrix. If the grains remained partly or completely surrounded by their host material (i.e., calcareous sandstone) for the entire burial period, then a  $D_e$  value of at least  $\sim 200$  Gy can be expected. But if they were disseminated among the archaeological sediments shortly after the latter were deposited, then the spalled grains

would have been exposed to a much higher dose rate for at least one-quarter of their burial time, so the  $D_e$  values may exceed  $\sim 300$  Gy. Any grain with a  $D_e$  of more than  $\sim 200$  Gy found in the samples collected from the cave sediments may, therefore, be derived from decomposed roof material and should be removed from the data set before final  $D_e$  and age determination.

We identified and rejected such grains by regenerating dose–response curves to  $\sim 400$  Gy, so that high  $D_e$  values associated with potentially spalled grains could be measured precisely. In many of the samples, these high  $D_e$  values form a discrete component centred on a  $D_e$  of 190–290 Gy (Fig. 4 and S5). Where present, this component is indicated as a grey line on the radial plots, and represents between 4% (SC2) and 23% (SC6) of the grains (Fig. S5). For contaminated samples, the presence of spalled grains holds significant implications for the use of multi-grain aliquots, which will result in age overestimates and/or less precise age estimates because of increased scatter in the  $D_e$  distributions. The advantage of single-grain OSL dating is that the removal of such grains from  $D_e$  data sets results in more accurate and precise estimates of depositional age.

#### 4.2. Contamination by younger intrusive grains

Eleven of the MP/MSA samples have  $D_e$  distributions that contain a small proportion of grains ( $<7\%$ ) that we interpret as younger intrusive grains. For ten of these samples, only few grains (1–8 grains) fall into this category, so their presence does not suggest large-scale mixing due to natural or anthropogenic processes. These few grains were omitted from the  $D_e$  data sets used to calculate the OSL ages.

Mixing presented a problem only for SC30, which is also the only sample collected from a context where MP/MSA deposits (in layer IV-2 in Sector IV) are directly overlain by deposits assigned to the Upper Paleolithic (layer 1b). The latter unconformably overlie the MP/MSA deposits at this location (Fig. 3e), but the nature of the erosional contact has not been established. Bioturbation by wasps is also pervasive in these deposits. Discrete  $D_e$  components could not be reliably fitted to the  $D_e$  distribution of SC30 (Fig. S5), which we think resulted from continuous sediment turnover for a prolonged period of time; mixing during the Upper Paleolithic is suggested by the smallest  $D_e$  values of  $\sim 20$  Gy, which correspond to ages of  $\sim 19$  ka. But given the obliteration of the integrity of this sample, a reliable age for the associated Aterian assemblage could not be calculated.

Sample SC30 can also be compared to sample OSL#7 of Schwenninger et al. (2010), which was collected from near the top of the section in Roche's Trench. They reported an age of  $59 \pm 10$  ka for this stratigraphically highest sample, but did not show the distribution of  $D_e$  values. The standard deviation of this  $D_e$  distribution can be deduced, however, from the standard error on the  $D_e$  estimate ( $52 \pm 8$  Gy) multiplied by the square root of the number of observations. Schwenninger et al. (2010) reported that they used between 6 and 18 aliquots per sample. This gives a standard deviation of between 20 Gy (6 aliquots) and 35 Gy (18 aliquots) at the 68% confidence interval, which corresponds to  $D_e$  values of between 10 and 90 Gy (6 aliquots) or between 0 and 120 Gy (18 aliquots) at the 95% confidence interval. This spread is consistent with that observed for single grains of SC30, which produced  $D_e$  values of 15–150 Gy, in addition to a roof spall component centred on  $\sim 250$  Gy (Fig. S5). Combining such widely scattered  $D_e$  values for multi-grain aliquots requires justification. Taking the average of the  $D_e$  values for a sediment mixture will give ages that are distorted by the (unknown) relative proportions and OSL intensities of grains in each mixing component. We argue, therefore, that evidence of the Aterian at Contrebandiers at  $\sim 60$  ka

(Schwenninger et al., 2010) should be disregarded, due to significant post-depositional disturbance in this part of the depositional sequence.

#### 4.3. Small-scale differences in beta dose rate

All but two of the Contrebandiers samples (SC4 and SC8) have typical 'scattered'  $D_e$  distributions (Jacobs et al., 2008a) that can be explained by small-scale differences in the beta dose delivered to individual grains. The methods used to establish whether a sample has been affected by beta microdosimetry variations, and the means of obtaining appropriate  $D_e$  values for age determination, are presented in Supplementary Material, together with worked examples. These samples have  $D_e$  distributions to which two discrete components can be fitted (indicated by the grey shaded bars on each of the radial plots in Fig. S5), after removing younger intrusive grains and older grains from decomposed roof spall (shown by grey lines in Fig. S5). The proportion of grains in the main  $D_e$  component is typically 70–90%, with 10–30% in the minor  $D_e$  component. Inhomogeneous spatial variations in the abundance of carbonate indurations, and the proximity of grains to these, may explain the between-sample differences in the component proportions. We argue against mixing as the mechanism responsible for these 'scattered'  $D_e$  distributions, because the  $D_e$  value of the minor component is consistently about half that of the main component, which is compatible with a reduction in beta dose rate due to carbonate cementation. In addition, the proportion of grains in the two components down profile is inconsistent with mixing as a result of particle diffusion, which would be expected to follow a function of exponential decay with increasing depth (Heimsath et al., 2002).

For these distributions, the  $D_e$  value of the main component (i.e., the  $D_e$  component containing the greatest proportion of grains) was used to calculate the sample age, after adjusting the beta dose rate using the approach described by Jacobs et al. (2008a); a worked example is presented in Supplementary Material.

### 5. Environmental dose rate measurements and results

The majority of the environmental dose rate—the denominator in the OSL age equation—is derived from beta particles and gamma rays emitted by the radioactive decay of  $^{238}\text{U}$ ,  $^{235}\text{U}$ ,  $^{232}\text{Th}$  (and their daughter products) and  $^{40}\text{K}$  in the sediments immediately surrounding the sample. There is also a smaller contribution from cosmic rays and from alpha particles internal to the quartz grains.

The beta dose rates for all samples were measured using a GM-25-5 low-level beta counter (Bøtter-Jensen and Mejdahl, 1988), making allowance for the effect of grain size (Mejdahl, 1979) and hydrofluoric acid etching (Bell and Zimmerman, 1978) on beta dose attenuation. This approach does not give information on whether the beta emissions originated from the U or Th decay chains, or from  $^{40}\text{K}$ , but instead gives the total counts from these sources. However, ~60% of the beta dose rate in the  $^{238}\text{U}$  series originates from decays in the lower part of the chain; determination of the beta dose rate in this way, therefore, does not depend critically on the assumptions of secular equilibrium in the  $^{238}\text{U}$  chain, which is commonly not the case (Olley et al., 1996, 1997). Where necessary, the beta dose rates were also adjusted for the effects of carbonate cementation, using the procedure described in Jacobs et al. (2008a). A worked example and discussion of the effects of this correction on the final age estimates is provided in Supplementary Material.

For 24 of the samples, gamma rays were measured *in situ* with a NaI(Tl) detector (which was inserted into the holes created when the OSL sample tubes were removed); this approach accounts for

any spatial heterogeneity in the gamma radiation field around each sample. The dose rates were determined using the "threshold" technique (Mercier and Falguères, 2007), which gives an estimate of the combined dose rate from gamma-ray emitters in the U and Th chains and from  $^{40}\text{K}$ . As with beta counting, this approach is much less sensitive to U-series disequilibria than are methods that calculate the gamma dose rate from the parental U concentrations, because ~98% of the gamma dose rate in the  $^{238}\text{U}$  series originates from decays in the lower part of the chain. For samples SC1–4, SC6–8, SC22 and SC26, the gamma dose rates were calculated using a combination of beta counting and thick-source alpha counting to obtain activity concentrations of U, Th and K, which were converted to dose rates (Adamiec and Aitken, 1998). No significant or systematic differences were observed between the gamma dose rates measured in these two ways for samples collected from adjacent squares (SC1–4 and SC10–13; Table 2). This provides further support that there are no significant problems associated with uranium disequilibria in our samples. By measuring the beta and gamma dose rates in these ways, we have implicitly assumed that the present state of (dis)equilibrium in the U and Th decay chains has prevailed throughout the period of sample burial. Numerical modelling has shown, however, that this assumption is unlikely to lead to errors in the total dose rate of more than 2–3%, even for the most common time-dependent disequilibria in the  $^{238}\text{U}$  series, when techniques such as those used in this study are employed (Olley et al., 1996, 1997).

The beta and gamma dose rates were corrected for the estimated long-term moisture content of each sample (Aitken, 1985). At the present day, the area above Contrebandiers is densely populated and artificially irrigated, so the cave sediments are unusually wet. The measured moisture contents of 3–25% (Table 2) are, therefore, considered unrepresentative of the long-term average water contents, and we opted to use a value of  $10 \pm 2.5\%$  for most of the Contrebandiers samples; the uncertainty is sufficient to accommodate the likely range of water contents averaged over the period of sample burial. This value is consistent with the moisture contents of the deposits in the nearby caves of El Mnasra and El Harhoura 2, which are less affected by modern irrigation (Jacobs et al., submitted for publication). For samples located outside the drip line (i.e., in Sector IV and the Roche Trench), we used the measured (field) moisture contents (Table 2). The total dose rates decrease, and the OSL ages increase, by ~1% for each 1% increase in water content.

An internal alpha dose rate of  $0.03 \pm 0.01$  Gy/ka was included in the total dose rate for all samples, based on previous measurements of acid-etched quartz grains from South and East Africa, and Australia (Feathers and Migliorini, 2001; Jacobs et al., 2003a; Bowler et al., 2003). The cosmic-ray dose rates were estimated from the equations provided by Prescott and Hutton (1994), taking into account the thickness, density and water content (Readhead, 1987) of deposit overlying each sample (averaged over the full period of burial), the thickness and density of rock overburden, and the altitude and geomagnetic latitude of the site. We also allowed for the configuration of the cave, by making a correction for the  $\cos^2\Phi$  zenith angular distribution of cosmic rays (Smith et al., 1997).

The total dose rate of the samples collected from the Mousterian and Aterian levels varies between  $0.78 \pm 0.04$  and  $1.27 \pm 0.08$  Gy/ka (Table 2), which is similar to the range of values reported for El Mnasra and El Harhoura 2 (Jacobs et al., submitted for publication). The dose rates of the samples collected from the uncemented sands at the base of the sediment profile (layer 7) are slightly lower (~0.60 Gy/ka), and lower still for the two bedrock samples (0.4–0.5 Gy/ka). For all samples, the uncertainty associated with the total dose rate represents the quadratic sum of all known and estimated sources of random and systematic error.

## 6. Age estimates and discussion

To obtain an age for each sample, the model-derived  $D_e$  value was divided by the beta-adjusted environmental dose rate. The assumptions involved in this adjustment procedure are not critical to the ages obtained. That is, use of the weighted mean  $D_e$  values (calculated after rejection of grains recognised as roof spall contamination and younger intrusive grains) divided by the bulk sample environmental dose rate give ages that are statistically indistinguishable (Table S5) from the FMM-derived ages presented in Table 2. But the latter are stratigraphically more coherent and take into account the extensive presence of carbonate in the deposit (Fig. S6–S8), so they are our preferred age estimates for Contrebandiers.

The  $D_e$  values, dose rates and single-grain ages are listed in Table 2 for all but one (SC30) of the Contrebandiers samples. Uncertainties on the ages are given at  $1\sigma$ , and were calculated by combining in quadrature the total uncertainties on the  $D_e$  and dose rate estimates. Also included is a systematic uncertainty of 2% to allow for possible bias in the calibration of the laboratory beta source.

The ages for the MP/MSA levels indicate that the sediments containing the Moroccan Mousterian and Aterian assemblages were deposited over a relatively short interval, between about 120 and 90 ka ago (Marine Isotope Stages 5d to 5b), following deposition of beach sands (layer 7) during the Last Interglacial (Marine Isotope Stage 5e).

To further resolve the chronology for the site, we used the statistical (homogeneity) test of Galbraith (2003) to determine if the independent ages from each layer or archaeological industry are self-consistent (i.e., the spread in ages for each layer is statistically compatible with the size of the age uncertainties). This test assumes that the OSL ages are independent observations sampled from a log-normal distribution, and the null hypothesis is that the ages are consistent with a common value. We expect a log-normal distribution of ages, rather than a Gaussian distribution, because the size of the age uncertainty is roughly proportional to sample age, whereas the size of the relative uncertainty is independent of age and can be closely approximated by using the log-transformed values (Galbraith, 2003). We recognise that this test should be used to compare multiple estimates of age for a specific event, whereas we are comparing age estimates for sediments possibly deposited over several centuries, millennia or longer. Such time intervals will be hard to discern if they are shorter than the size of the individual age uncertainties. In the present context, therefore, we are using the homogeneity test to establish if the spread in ages is sufficiently narrow that the null hypothesis cannot be rejected when the age uncertainties are taken into account. The latter outcome would indicate that the ages of the relevant layer or archaeological industry are consistent with either a single event or with sediment accumulation over a time span commensurate with the size of the age uncertainties (i.e., several millennia at  $1\sigma$ ).

The calculated  $P$ -values (which indicate the probability that a random value from a chi-squared distribution with  $n-1$  degrees of freedom is greater than the homogeneity test statistic,  $G$ ) are listed in Table 3, alongside the individual ages for each sample in the different groups. A small  $P$ -value (by convention  $<0.05$ ) indicates that the ages are not all compatible with a common value. The  $P$ -values for each group are significantly greater than 0.05, which supports the null hypothesis and suggests that the OSL ages are self-consistent within each group. Accordingly, we calculated a weighted mean age for each layer or industry (Table 3), under the assumption that the individual ages represent either a single event or a series of events spread over a time interval that is short compared to the size of the age uncertainties. More sophisticated statistical models (e.g., Jacobs et al., 2008c) may be able to

**Table 3**

OSL ages for each sample dated from Contrebandiers. Also shown are the calculated  $P$ -values (used to assess whether the ages obtained for samples associated with each industry are statistically self-consistent) and the weighted mean OSL ages for the different industries and archaeological layers.

Sample name	OSL age (ka)	$P$ -value	Weighted mean OSL age (ka)	$P$ -value and grand weighted mean OSL age (ka)
Aterian (Roche Trench and layer IV-2 in Sector IV)				
SC30	Indeterminate			
SC39	96 ± 8	0.71	95.9 ± 4.1	$P = 0.42$
SC37	101 ± 9			103.2 ± 3.0
SC31	92 ± 6			
SC32	97 ± 7			
Aterian (layer 4 in the central excavation area and layer V-1b and V-2 in Sector V)				
SC21	103 ± 6	0.78	107.4 ± 3.5	
SC35	105 ± 9			
SC20	104 ± 7			
SC8	108 ± 9			
SC7	117 ± 9			
SC23	113 ± 7			
SC34	107 ± 9			
Moroccan Mousterian (layers 5a–c)				
SC16	118 ± 9	0.98	115.3 ± 3.4	$P = 0.92$
SC15	116 ± 8			116.1 ± 2.9
SC19	124 ± 9			
SC14	113 ± 7			
SC6	114 ± 8			
SC13	112 ± 7			
SC1	115 ± 8			
SC28	115 ± 8			
SC2	114 ± 8			
Archaeologically sterile (layers 6a/b)				
SC18	114 ± 6	0.98	112.2 ± 4.2	
SC29	109 ± 7			
SC12	119 ± 8			
SC3	107 ± 8			
Moroccan Mousterian (layer 6c)				
SC11	122 ± 9	0.78	122.3 ± 4.5	
SC17	119 ± 7			
SC4	120 ± 8			
SC10	130 ± 9			
Archaeologically sterile (layer 7)				
SC5	123 ± 11	0.70	126.4 ± 9.1	
SC9	132 ± 15			

distinguish between these options, but we note that the oldest and youngest individual ages for each layer or industry are consistent with the weighted mean, so our conclusions should be robust. Before calculating the  $P$ -values, we removed the 2% systematic uncertainty, but we have added this (in quadrature) to each of the weighted mean errors to obtain the total uncertainties listed in Table 3.

The weighted mean OSL ages provide a chronological sequence of improved precision for the MP/MSA layers at Contrebandiers. An age of  $126 \pm 9$  ka is obtained for the basal sand unit (layer 7), consistent with deposition during the Last Interglacial sea-level highstand. An age of  $122 \pm 5$  ka is calculated for the earliest Moroccan Mousterian in layer 6c, and the overlying, archaeologically sterile, layer 6a/b is dated to  $112 \pm 4$  ka. This layer is directly overlain by the densest Moroccan Mousterian deposits (layers 5a–c), which have a weighted mean age of  $115 \pm 3$  ka. The earliest occurrence of Aterian at the site (layers 4c and d and Sector V) is dated to  $107 \pm 4$  ka, and the latest occurrence of the Aterian (in Sector IV and the Roche Trench) has a weighted mean age of  $96 \pm 4$  ka. These two Aterian ages are significantly different at  $2\sigma$ : that is, they differ by  $11 \pm 5$  ka, where the uncertainty is calculated as the square root of the sum of squared weighted mean errors (with the 2% systematic uncertainty removed). This indicates that the Aterian industry may have lasted for up to 20 ka at this site.

**Table 4**

Comparison of ages obtained in this study with those in Schwenninger et al. (2010). The current excavation team have correlated the Roche stratigraphy (used by Schwenninger et al., 2010) with their stratigraphy (used in this study) to facilitate direct comparisons.

Stratigraphic layers in central excavation area	Schwenninger et al. (2010)			This study		Mean ratio (Column 4/Column 6)
	Sample name	Roche stratigraphy	Age (ka)	Sample name	Age (ka)	
4d	OSL#6	9/10	100 ± 8	SC32	97 ± 7	0.96 ± 0.12
	OSL#8		99 ± 11	SC31	92 ± 6	
				SC20	104 ± 7	
				SC8	108 ± 9	
				SC7	117 ± 9	
5b	OSL#5	11b	106 ± 10	SC15	116 ± 8	0.91 ± 0.11
5c	OSL#4	11c	105 ± 8	SC19	124 ± 9	0.84 ± 0.11
	OSL#9		96 ± 14	SC14	113 ± 7	
				SC6	114 ± 8	
				SC13	112 ± 7	
				SC1	115 ± 8	
				SC2	114 ± 8	
				SC28	115 ± 8	
6a/b	OSL#3	13a–c	100 ± 10	SC18	114 ± 6	0.90 ± 0.11
				SC29	109 ± 7	
				SC12	119 ± 8	
				SC3	107 ± 8	
6c	OSL#2	13d	122 ± 14	SC11	122 ± 9	1.02 ± 0.11
	OSL#1	14/15	129 ± 7	SC17	119 ± 7	
				SC4	120 ± 8	
				SC10	130 ± 9	

To further improve the precision of the age estimate for the Moroccan Mousterian at Contrebandiers, we combined all ages obtained for layers 5 and 6 and calculated a grand weighted mean of  $116 \pm 3$  ka (listed in the final column of Table 3). We did likewise for the Aterian samples and obtained a grand weighted mean of  $103 \pm 3$  ka. In both cases, the *P*-values indicate that the individual age estimates are consistent with a common value (Table 3), although we note that the Aterian ages from Sector IV and the Roche Trench are systematically younger than those from the central excavation area and Sector V. These two grand weighted mean ages are significantly different at  $2\sigma$  and provide statistical support for a possible hiatus of  $13 \pm 3$  ka (calculated as above) between the Moroccan Mousterian and Aterian at Contrebandiers. If the comparison is made, instead, between the grand weighted mean for the Mousterian (or the weighted mean for the latest Mousterian) and the weighted mean for the earliest Aterian, then a statistically significant hiatus of  $9 \pm 3$  ka (or  $8 \pm 4$  ka) is determined. These two industries, therefore, may be distinct time entities at Contrebandiers (i.e., separated chronologically), but whether or not they are technologically (i.e., archaeologically) distinct is currently under investigation.

Overall, our single-grain OSL chronology confirms the age estimates obtained previously for MP/MSA assemblages at Contrebandiers and other sites in the vicinity (Barton et al., 2009; Schwenninger et al., 2010; Jacobs et al., submitted for publication). Table 4 provides a comparison of the ages obtained in this study with those reported for Contrebandiers by Schwenninger et al. (2010). They obtained ages using between 6 and 18 aliquots per sample, where each aliquot consisted of 50–150 sand-sized grains of quartz. The determination of  $D_e$  values and OSL ages from such large aliquots is apt to conceal details of the post-depositional history of a sample, by averaging out the effects of contamination by older and younger grains. In this study, we have demonstrated that contamination of the archaeological deposits by unbleached grains derived from disintegrated roof spall is a particularly acute problem for the majority of samples examined from this site. Multi-grain aliquots can also give rise to inaccurate  $D_e$  estimates (and, hence, OSL ages) if they contain grains with aberrant OSL behaviours. A large proportion of grains measured in

this study exhibited such behaviours (Table S1), and had to be rejected prior to  $D_e$  and age determination.

The current excavation team has correlated the previously published stratigraphy of Roche (used by Schwenninger et al., 2010) with the stratigraphy recorded during the most recent excavations. This permits a direct comparison of the ages produced in both OSL dating studies. Overall, the ages obtained for the same layers are statistically consistent. Unfortunately, Schwenninger et al. (2010) provide no information about the  $D_e$  distributions of their samples that would enable us to assess the validity of their age estimates, but it can be deduced from the size of the uncertainties on the  $D_e$  values that the latter must be considerably overdispersed. When such large overdispersion is observed for multi-grain aliquots, then it may not be valid to combine the individual  $D_e$  values to obtain a (weighted) mean estimate. By contrast, our single-grain OSL ages are more precise and less scattered than the ages reported by Schwenninger et al. (2010), which we attribute to the advantages inherent in analysing individual grains of quartz.

## 7. Concluding remarks

The MP/MSA deposits at Contrebandiers provide further insights into the timing and duration of the Moroccan Mousterian and Aterian in western Morocco. By measuring and analysing the OSL signals from individual sand-sized grains of quartz, it has proven possible to obtain reproducible and accurate OSL ages. The single-grain OSL chronology suggests that the site was occupied for a relatively short interval between MIS 5d and 5b, and that the Moroccan Mousterian and Aterian represent distinct time entities at Contrebandiers, separated by an occupational hiatus of up to  $13 \pm 3$  ka.

To answer questions about durations, gaps or continuities in the archaeological record, and to make correlations with other (e.g., palaeoenvironmental) archives, it is imperative to understand the depositional and post-depositional history of the sediments. This can only be achieved using OSL dating if  $D_e$  values are measured for individual grains and the resulting distributions are analysed by combining appropriate statistical techniques with a thorough knowledge of sample context. By adopting this approach, we have

obtained ages of improved accuracy and precision for the MP/MSA industries at Contrebandiers. Further statistical modelling, such as that used by Jacobs et al. (2008c) or Barton et al. (2009), might provide more refined estimates of the duration of MP/MSA occupation of Contrebandiers and the timing of the gaps or transitions between the major industries.

## Acknowledgements

The project at Contrebandiers is a joint Moroccan–American project under the auspices of the Moroccan Institut National des Sciences de l'Archéologie et du Patrimoine. The majority of this research was funded by the Australian Research Council through Discovery Project grants DP0666084 to Roberts and Jacobs and DP1092843 to Jacobs and Dibble and by the National Science Foundation (0935491), with other contributions from the Leakey Foundation, the National Geographic Society, and the University Research Foundation of the University of Pennsylvania. Meyer was funded by the Seventh Framework Programme of the European Union (grant IOF-GEOPAL-219944). We would like to thank all members of the excavation and research teams for valuable information that has helped us to understand and interpret the OSL data, and the five reviewers for their comments.

## Appendix. Supplementary material

Supplementary material associated with this article can be found, in the online version, at doi:10.1016/j.jas.2011.08.033.

## References

- Adamiec, G., Aitken, M., 1998. Dose-rate conversion factors: update. *Ancient TL* 16, 37–50.
- Aitken, M.J., 1985. *Thermoluminescence Dating*. Academic Press, London.
- Arnold, L.J., Roberts, R.G., 2009. Stochastic modelling of multi-grain equivalent dose ( $D_e$ ) distributions: implications for OSL dating of sediment mixtures. *Quaternary Geochronology* 4, 204–230.
- Balter, M., 2011. Was North Africa the launch pad for modern human migration? *Science* 331, 20–23.
- Barton, R.N.E., Bouzouggar, A., Collcutt, S.N., Schwenninger, J.-L., Clark-Balzan, L., 2009. OSL dating of the Aterian levels at Dar es-Soltan I (Rabat, Morocco) and implications for the dispersal of modern *Homo sapiens*. *Quaternary Science Reviews* 28, 1914–1931.
- Bateman, M.D., Frederick, C.D., Jaiswal, M.K., Singhvi, A.K., 2003. Investigations into the potential effects of pedoturbation on luminescence dating. *Quaternary Science Reviews* 22, 1169–1176.
- Bateman, M.D., Boulter, C.H., Carr, A.S., Frederick, C.D., Peter, D., Wilder, M., 2007a. Detecting post depositional sediment disturbance in sandy deposits using optical luminescence. *Quaternary Geochronology*, 57–64.
- Bateman, M.D., Boulter, C.H., Carr, A.S., Frederick, C.D., Peter, D., Wilder, M., 2007b. Preserving the palaeoenvironmental record in Drylands: bioturbation and its significance for luminescence-derived chronologies. *Sedimentary Geology* 195, 5–19.
- Bell, W.T., Zimmerman, D.W., 1978. The effect of HF acid etching on the morphology of quartz inclusions for thermoluminescence dating. *Archaeometry* 20, 63–65.
- Bøtter-Jensen, L., Mejdahl, V., 1988. Assessment of beta dose-rate using a GM multiscaler system. *Nuclear Tracks and Radiation Measurements* 14, 187–191.
- Bouzouggar, A., 1997a. Matières premières, processus de fabrication et de gestion des supports d'outils dans la séquence atérienne de la grotte des Contrebandiers à Témara (Maroc). Université Bordeaux I, Bordeaux.
- Bouzouggar, A., 1997b. Économie des matières premières et du débitage dans la séquence atérienne de la grotte d'El Mnasra I (Ancienne grotte des Contrebandiers – Maroc). *Préhistoire anthropologie méditerranéennes* 6, 35–52.
- Bouzouggar, A., Barton, N., Vanhaeren, M., d'Errico, F., Collcutt, S., Higham, T., Hodge, E., Parfitt, S., Rhodes, E., Schwenninger, J.L., Stringer, C., Turner, E., Ward, S., Moutmir, A., Stambouli, A., 2007. 82,000-year-old shell beads from North Africa and implications for the origins of modern human behaviour. *Proceedings of the National Academy of Sciences of the USA* 104, 9964–9969.
- Bowler, J.M., Johnston, H., Olley, J.M., Prescott, J.R., Roberts, R.G., Shawcross, W., Spooner, N.A., 2003. New ages for human occupation and climatic change at Lake Mungo, Australia. *Nature* 421, 837–840.
- David, B., Roberts, R.G., Magee, J., Mialanes, J., Turney, C., Bird, M., White, C., Fifield, L.K., Tibby, J., 2007. Sediment mixing at Nonda Rock: investigations of stratigraphic integrity at an early archaeological site in northern Australia and implications for the human colonisation of the continent. *Journal of Quaternary Science* 22, 449–479.
- Debénath, A., 2000. Le peuplement préhistorique du Maroc: données récentes et problèmes. *L'Anthropologie* 104, 131–145.
- Delibrias, G., Guillaud, M.T., Labeyrie, J., 1982. GIF natural radiocarbon measurements IX. *Radiocarbon* 24, 291–343.
- d'Errico, F., Vanhaeren, M., Barton, N., Bouzouggar, A., Mienis, H., Richter, D., Hublin, J.-J., McPherron, S.P., Lozouet, P., 2009. Additional evidence on the use of personal ornaments in the Middle Paleolithic of North Africa. *Proceedings of the National Academy of Sciences of the USA* 106, 16051–16056.
- Duller, G.A.T., Murray, A.S., 2000. Luminescence dating of sediments using individual mineral grains. *Geology* 5, 88–106.
- Duller, G.A.T., Bøtter-Jensen, L., Murray, A.S., 2000. Optical dating of single sand-sized grains of quartz: sources of variability. *Radiation Measurements* 32, 453–457.
- Feathers, J.K., Migliorini, E., 2001. Luminescence dating at Katanda – a reassessment. *Quaternary Science Reviews* 20, 961–966.
- Feathers, J.K., Rhodes, E., Huot, S., McAvoy, J., 2006a. Luminescence dating of sand deposits related to late Pleistocene human occupation at the Cactus Hill site, Virginia, USA. *Quaternary Geochronology* 1, 167–187.
- Feathers, J.K., Holliday, V.T., Meltzer, D.J., 2006b. OSL dating of Southern High Plains archaeological sites. *Journal of Archaeological Science* 33, 1651–1665.
- Feathers, J.K., Piló, L., Arroyo-Kalin, M., Kipnes, R., Coblenz, D., 2010. How old is Luzia? Luminescence dating and stratigraphic integrity at Lapa Vermelha, Lagoa Santa, Brazil. *Geoarchaeology* 25, 395–436.
- Ferembach, D., 1976. Les restes humains Atérien de Temara (Campagne 1975). *Bulletin Mémoires de la Société d'Anthropologie de Paris* 13, 175–180.
- Ferembach, D., 1998. La crâne Atérien de Témara (Maroc Atlantique). *Bulletin d'Archéologie marocaine* 18, 19–66.
- Galbraith, R.F., 1988. Graphical display of estimates having differing standard errors. *Technometrics* 30, 271–281.
- Galbraith, R.F., Roberts, R.G., Laslett, G.M., Yoshida, H., Olley, J.M., 1999. Optical dating of single grain and multiple grains of quartz from Jinnium rock shelter, Northern Australia: part I, experimental design and statistical models. *Archaeometry* 41, 339–364.
- Galbraith, R.F., 2003. A simple homogeneity test for estimates of dose obtained using OSL. *Ancient TL* 21, 75–77.
- Haslam, M., Roberts, R.G., Shipton, C., Pal, J.N., Fenwick, J.L., Ditchfield, P., Boivin, N., Dubey, A.K., Gupta, M.C., Petraglia, M., 2011. Late Acheulean hominins at the Marine Isotope Stage 6/5e transition in north-central India. *Quaternary Research* 75, 670–682.
- Heimsath, A.M., Chappell, J., Spooner, N.A., Questiaux, D.G., 2002. Creeping soil. *Geology* 30, 111–114.
- Hublin, J.-J., 1992. Recent human evolution in northwest Africa. *Philosophical Transactions of the Royal Society of London* 337, 185–191.
- Hublin, J.-J., 1993. Recent human evolution in northwestern Africa. In: Aitken, M., Stringer, C., Mellars, P. (Eds.), *The Origin of Modern Humans and the Impact of Chronometric Dating*. Princeton University Press, Princeton, pp. 118–131.
- Jacobs, Z., Wintle, A.G., Duller, G.A.T., 2003a. Optical dating of dune sand from Blombos Cave, South Africa: I – multiple grain data. *Journal of Human Evolution* 44, 599–612.
- Jacobs, Z., Duller, G.A.T., Wintle, A.G., 2003b. Optical dating of dune sand from Blombos Cave, South Africa: II – single grain data. *Journal of Human Evolution* 44, 613–625.
- Jacobs, Z., Duller, G.A.T., Wintle, A.G., 2006a. Interpretation of single grain  $D_e$  distributions and calculation of  $D_e$ . *Radiation Measurements* 41, 264–277.
- Jacobs, Z., Duller, G.A.T., Wintle, A.G., Henshilwood, C.S., 2006b. Extending the chronology of deposits at Blombos Cave, South Africa, back to 140 ka using optical dating of single and multiple grains of quartz. *Journal of Human Evolution* 51, 255–273.
- Jacobs, Z., Roberts, R.G., 2007. Advances in optically stimulated luminescence dating of individual grains of quartz from archaeological deposits. *Evolutionary Anthropology* 16, 210–223.
- Jacobs, Z., Wintle, A.G., Roberts, R.G., Duller, G.A.T., 2008a. Equivalent dose distributions from single grains of quartz at Sibudu, South Africa: context, causes and consequences for optical dating of archaeological deposits. *Journal of Archaeological Science* 35, 1808–1820.
- Jacobs, Z., Wintle, A.G., Duller, G.A.T., Roberts, R.G., Wadley, L., 2008b. New ages for the post-Howiesons Poort, late and final Middle Stone Age at Sibudu, South Africa. *Journal of Archaeological Science* 35, 1790–1807.
- Jacobs, Z., Roberts, R.G., Galbraith, R.F., Deacon, H.J., Grün, R., Mackay, A., Mitchell, P., Vogelsang, R., Wadley, L., 2008c. Ages for the Middle Stone Age of southern Africa: implications for human behavior and dispersal. *Science* 322, 733–735.
- Jacobs, Z., Roberts, R.G., Nespoulet, R., Debénath, A., El Hajraoui, M.A., Single-grain chronologies for Middle Palaeolithic deposits at El Mnasra and El Harhoura 2, Morocco: implications for Late Pleistocene human-environment interactions in northwestern Africa. *Journal of Human Evolution*, Submitted for publication.
- Lombard, M., Wadley, L., Jacobs, Z., Mohapi, M., Roberts, R.G., 2010. Still Bay and serrated points from Umhlatuzana Rock Shelter, Kwazulu-Natal, South Africa. *Journal of Archaeological Science* 37, 1773–1784.
- Marean, C.W., Bar-Matthews, M., Bernatchez, J., Fisher, E., Goldberg, P., Herries, A.I.R., Jacobs, Z., Jerardino, A., Karkanas, P., Minichillo, T., Nilssen, P.J., Thompson, E., Watts, I., Williams, H.M., 2007. Early human use of marine resources and pigment in South Africa during the Middle Pleistocene. *Nature* 449, 905–908.

- Ménard, J., 1998. Odontologie des dents de la grotte de Temara (Maroc). *Bulletin d'Archéologie Marocaine* 18, 67–97.
- Mejdahl, V., 1979. Thermoluminescence dating: beta-dose attenuation in quartz grains. *Archaeometry* 21, 61–72.
- Mercier, N., Falguères, C., 2007. Field gamma dose-rate measurement with a NaI(Tl) detector: re-evaluation of the “threshold” technique. *Ancient TL* 25, 1–4.
- Murray, A.S., Roberts, R.G., 1997. Determining the burial time of single grains of quartz using optically stimulated luminescence. *Earth and Planetary Science Letters* 152, 163–180.
- Murray, A.S., Olley, J.M., 2002. Precision and accuracy in the optically stimulated luminescence dating of sedimentary quartz: a status review. *Geochronometria* 21, 1–16.
- Olley, J.M., Murray, A., Roberts, R.G., 1996. The effects of disequilibria in the uranium and thorium decay chains on burial dose rates in fluvial sediments. *Quaternary Science Reviews* 15, 751–760.
- Olley, J.M., Roberts, R.G., Murray, A.S., 1997. Disequilibria in the uranium decay series in sedimentary deposits at Allen's Cave, Nullarbor Plain, Australia: implications for dose rate determinations. *Radiation Measurements* 27, 433–443.
- Olley, J.M., Caitcheon, G.G., Roberts, R.G., 1999. The origin of dose distributions in fluvial sediments, and the prospect of dating single grains from fluvial deposits using optically stimulated luminescence. *Radiation Measurements* 30, 207–217.
- Olley, J.M., Pietsch, T., Roberts, R.G., 2004. Optical dating of Holocene sediments from a variety of geomorphic settings using single grains of quartz. *Geomorphology* 60, 337–358.
- Olley, J.M., Roberts, R.G., Yoshida, H., Bowler, J.M., 2006. Single-grain optical dating of grave-infill associated with human burials at Lake Mungo, Australia. *Quaternary Science Reviews* 25, 2469–2474.
- Porat, N., Rosen, S.A., Boaretto, E., Avni, Y., 2006. Dating the Ramat Saharonim late Neolithic desert cult site. *Journal of Archaeological Science* 33, 1341–1355.
- Prescott, J.R., Hutton, J.T., 1994. Cosmic ray contributions to dose rates for luminescence and ESR dating: large depths and long term time variations. *Radiation Measurements* 23, 497–500.
- Readhead, M.L., 1987. Thermoluminescence dose rate data and dating equations for the case of disequilibrium in the decay series. *Nuclear Tracks and Radiation Measurements* 13, 197–207.
- Richter, D., Moser, J., Nami, M., Eiwanger, J., Mikdad, A., 2010. New chronometric data from Ifri n'Ammar (Morocco) and the chronostratigraphy of the Middle Palaeolithic in the Western Maghreb. *Journal of Human Evolution* 59, 672–679.
- Roberts, R.G., Bird, M., Olley, J., Galbraith, R., Lawson, E., Laslett, G., Yoshida, H., Jones, R., Fullagar, R., Jacobsen, G., Hua, Q., 1998. Optical and radiocarbon dating at Jinmium rock shelter in northern Australia. *Nature* 393, 358–362.
- Roberts, R.G., Galbraith, R.F., Olley, J.M., Yoshida, H., Laslett, G.M., 1999. Optical dating of single and multiple grains of quartz from Jinmium rock shelter, northern Australia: part II, results and implications. *Archaeometry* 41, 365–395.
- Roberts, R.G., Galbraith, R.F., Yoshida, H., Laslett, G.M., Olley, J.M., 2000. Distinguishing dose populations in sediment mixtures: a test of single-grain optical dating procedures using mixtures of laboratory-dosed quartz. *Radiation Measurements* 32, 459–465.
- Roche, J., 1958–1959. L'Épipaléolithique Marocain. *Libyca* 6–7, 159–192.
- Roche, J., 1963. L'Épipaléolithique Marocaine. *Fondation Calouste Gulbenkian, Lisbon*.
- Roche, J., 1976. Chronostratigraphie des restes atériens de la grotte des Contrebandiers à Témara (Province de Rabat). *Bulletins et Mémoires de la Société d'Anthropologie de Paris*, 165–173.
- Roche, J., Texier, J.-P., 1976. Découverte de restes humains dans un niveau atérien supérieur de la grotte des Contrebandiers, à Temara (Maroc). *C.R. Académie des Sciences* 282, 45–47.
- Schurmans, U., Dibble, H., El Hajraoui, M.A., 2007. Archaeological Excavations of Smugglers' Cave, Temara. Report of the 2007 Excavation Season. Interim Field Report. University of Pennsylvania, Philadelphia & Ministère de la Culture, Rabat.
- Schurmans, U., Dibble, H., El Hajraoui, M.A., 2009. Archaeological Excavations of Smugglers Cave', Temara. Report of the 2008 Excavation Season. Interim Field Report. University of Pennsylvania, Philadelphia & Ministère de la Culture, Rabat.
- Schwenninger, J.-L., Collcutt, S.N., Barton, N., Bouzouggar, A., Clark Balzan, L., El Hajraoui, M.A., Nespoulet, R., Debénath, A., 2010. A new luminescence chronology for Aterian cave sites on the Atlantic coast of Morocco. In: Garcea, E.A. (Ed.), *South-Eastern Mediterranean Peoples between 130,000 and 10,000 years ago*. Oxbow Books, Oxford, pp. 18–36.
- Smith, M.A., Prescott, J.R., Head, M.J., 1997. Comparison of <sup>14</sup>C and luminescence chronologies at Puritjarra rock shelter, central Australia. *Quaternary Science Reviews* 16, 299–320.
- Smith, T.M., Tafforeau, P., Reid, D.J., Grün, R., Eggers, S., Boutakiout, M., Hublin, J.-J., 2007. Earliest evidence of modern human life history in North African early Homo sapiens. *Proceedings of the National Academy of Sciences of the USA* 104, 6128–6133.
- Tribolo, C., Mercier, N., Rasse, M., Soriano, S., Huysecom, E., 2010. Kobo 1 and L'Abri aux Vaches (Mali, West Africa): two case studies for the optical dating of bioturbated sediments. *Quaternary Geochronology* 5, 317–323.
- Yoshida, H., Roberts, R.G., Olley, J.M., Laslett, G.M., Galbraith, R.F., 2000. Extending the age range of optical dating using single 'supergrains' of quartz. *Radiation Measurements* 32, 439–446.